LETTER

doi:10.1038/nature12151

Chemical mapping of a single molecule by plasmon-enhanced Raman scattering

R. Zhang[1]*, Y. Zhang[1]*, Z. C. Dong[1], S. Jiang[1], C. Zhang[1], L. G. Chen[1], L. Zhang[1], Y. Liao[1], J. Aizpurua[2], Y. Luo[1,3], J. L. Yang[1] & J. G. Hou[1]

Visualizing individual molecules with chemical recognition is a longstanding target in catalysis, molecular nanotechnology and biotechnology. Molecular vibrations provide a valuable 'fingerprint' for such identification. Vibrational spectroscopy based on tip-enhanced Raman scattering allows us to access the spectral signals of molecular species very efficiently via the strong localized plasmonic fields produced at the tip apex[1–11]. However, the best spatial resolution of the tip-enhanced Raman scattering imaging is still limited to 3–15 nanometres[5,12–16], which is not adequate for resolving a single molecule chemically. Here we demonstrate Raman spectral imaging with spatial resolution below one nanometre, resolving the inner structure and surface configuration of a single molecule. This is achieved by spectrally matching the resonance of the nanocavity plasmon to the molecular vibronic transitions, particularly the downward transition responsible for the emission of Raman photons. This matching is made possible by the extremely precise tuning capability provided by scanning tunnelling microscopy. Experimental evidence suggests that the highly confined and broadband nature of the nanocavity plasmon field in the tunnelling gap is essential for ultrahigh-resolution imaging through the generation of an efficient double-resonance enhancement for both Raman excitation and Raman emission. Our technique not only allows for chemical imaging at the single-molecule level, but also offers a new way to study the optical processes and photochemistry of a single molecule.

Chemical identification by optical means down to single-molecule sensitivity is a challenging task and usually requires large enhancements of the local fields acting on the molecule[6,7,17–19]. These field enhancements can typically be achieved by using metallic nanoparticles acting as optical antennas to increase the signals[8,11,17,19]. One of the most efficient optical antennas consists of a metallic tip that localizes and enhances optical fields at the tip apex, as in tip-enhanced Raman scattering (TERS), enabling a combination of spectroscopy and microscopy capabilities[1–8,12–18]. However, the spatial extent of the local plasmonic field (5–10 nm) appears to be a limiting factor for spatial resolution[18,20]. Moreover, conventional TERS usually requires the use of strong incident laser fields that could result in undesired diffusion, desorption and even damage to the molecule, thus affecting the sustainability and stability of Raman spectral mapping.

Here we present an experimental study of plasmon-enhanced Raman imaging of single molecules located at the scanning tunnelling microscopy (STM) nanocavity under ultrahigh vacuum and low temperature

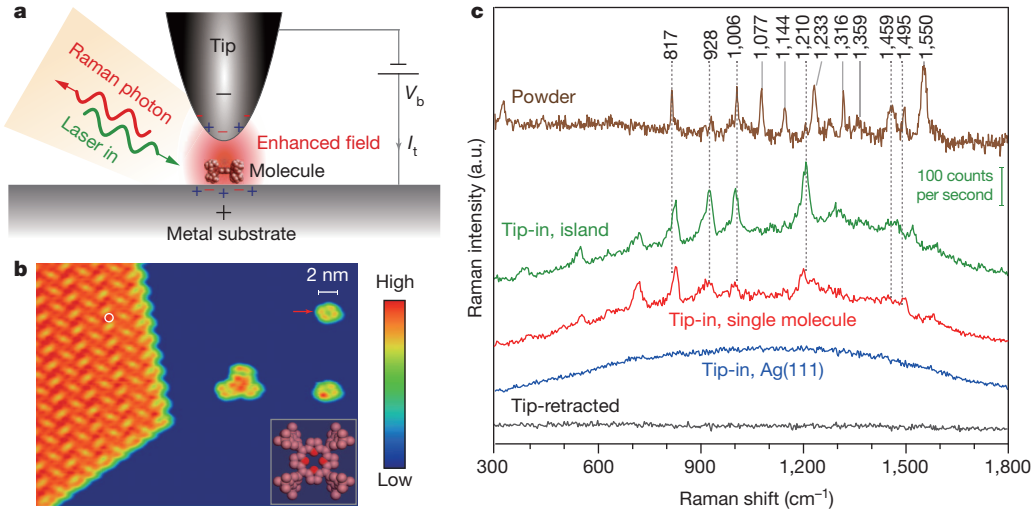

Figure 1 | Clean TERS spectra using well-defined tip and sample. **a**, Schematic tunnelling-controlled TERS in a confocal-type side-illumination configuration, in which V_b is the sample bias and I_t is the tunnelling current. **b**, STM topograph of sub-monolayered H_2TBPP molecules on Ag(111) (1.5 V, 30 pA, 35 nm × 27 nm). The inset shows the chemical structure of H_2TBPP and the white circle indicates one representative site for TERS measurements on the molecular islands. **c**, TERS spectra for different conditions. The tip-in spectra were acquired at 120 mV, 0.5 nA and 3 s. The green spectrum is taken on top of the molecular island (the green scale bar shows the signal level detected by charge-coupled device (CCD). The red spectrum is taken on top of a single molecule (marked by the red arrow in **b**). The blue spectrum is taken on bare Ag(111). The black spectrum is taken on top of the molecular island but with the tip retracted 5 nm from the surface (120 mV, 3 s). For comparison, a standard Raman spectrum (brown) is shown on the top for a powder sample of H_2TBPP molecules.

[1]Hefei National Laboratory for Physical Sciences at the Microscale, University of Science and Technology of China, Hefei, Anhui 230026, China. [2]Material Physics Center CSIC-UPV/EHU and Donostia International Physics Center DIPC, Paseo Manuel de Lardizabal 5, Donostia-San Sebastián 20018, Spain. [3]Theoretical Chemistry and Biology, School of Biotechnology, Royal Institute of Technology, S-10691 Stockholm, Sweden.
*These authors contributed equally to this work.

(Fig. 1a and Supplementary Fig. 1). These special conditions allow us to achieve exquisite tuning between the nanocavity plasmon (or tip plasmon) resonance and the molecular vibronic transitions. In particular, the spectral matching of the nanocavity plasmon resonance to the downward transitions associated with the emission of Raman photons is found to be crucial for enhancing and stabilizing the inelastic scattering signals. Remarkably, the very small incident photon flux used in our STM-controlled spectral-matching TERS enables stable single-molecule mapping with unambiguous chemical identification and unprecedented sub-molecular spatial resolution for a single *meso*-tetrakis(3,5-di-tertiarybutylphenyl)-porphyrin (H_2TBPP) molecule on the Ag(111) surface.

Figure 1b and c illustrate the high quality and level of cleanness of the tip and sample under a low-temperature and ultrahigh-vacuum environment[13,17,21], which allows for reproducible chemical identifications through vibrational fingerprints. In the STM image of Fig. 1b for H_2TBPP on Ag (111), we can identify two isolated single molecules on the right (featuring the characteristic four-lobe pattern[22,23]), a three-molecule cluster at the centre, and a densely packed monolayer island on the left. The bare Ag surface in blue serves as an *in situ* checkground for monitoring the tip cleanness and the nanocavity plasmon resonance mode.

As shown in Fig. 1c, when a tip is positioned on the bare Ag surface, a featureless spectrum (blue) containing simply a broad continuum is obtained, consistent with the absence of molecules and also suggesting the operation of a contamination-free tip. On top of the molecular islands (marked with a white circle in Fig. 1b), the TERS spectrum (green) shows clear vibrational fingerprints of H_2TBPP molecules over a broad continuum. The spectral features do not change substantially when acquired at different positions of molecules on the island (Supplementary Fig. 2). When the tip is retracted about 5 nm from the island (black spectrum), the molecular fingerprints disappear, providing unambiguous evidence that the TERS signals observed in the green spectrum originate only from the molecular sample itself. The far-field Raman signal associated with the tip-retracted mode is absent, so a relatively high signal-to-noise ratio for the TERS signal (for example, the 1,210 cm^{-1} peak) implies a large enhancement in the present system[17,18]. This is nicely illustrated by the TERS measurements on an isolated single H_2TBPP molecule (red spectrum), which exhibits unambiguous vibrational fingerprints similar to those on the molecular island.

We note that inelastic electron tunnelling spectroscopy in cryogenic STM can also provide information about certain vibrational modes of a single molecule through inelastic electron exication[24]. By contrast, the STM-controlled TERS provides full vibrational fingerprints of molecules through the excitation of optical fields alone. Localized tunnelling electrons do not contribute to the TERS signals because the vibrational fingerprints of the H_2TBPP molecule show up in the spectrum even when the bias voltage is well below the excitation threshold of vibrational modes (see Supplementary Fig. 3 and related discussion in the Supplementary Information).

For comparison, the standard Raman signals from a H_2TBPP powder sample are also given in Fig. 1c, showing all Raman-active modes averaged over the full space of randomly oriented molecules. Many of the fingerprint peaks of the powder spectrum are in good correspondence with the vibrational fingerprints on the molecular island and single molecules (see dashed lines), thus providing clear chemical identification of the molecules on the surface. However, the number and relative intensity of peaks reveal differences as well. These could be attributed to the ordering of the H_2TBPP molecules on Ag(111) and the preferred axial polarization of the nanocavity plasmon, which selects particular Raman modes. A detailed spectral assignment is given in the Supplementary Methods and Supplementary Video, obtained using density functional theory calculations.

Of particular interest is the broad continuum that usually accompanies the TERS measurements on both the bare metal surface and the molecules (Fig. 1c)[25–27]. This broad continuum turns out to correlate closely with the nanocavity plasmon resonance mode that is determined by the junction geometry of the STM nanocavity and dielectric properties of the tip and substrate[25], and can be monitored *in situ* by STM-induced luminescence through tunnelling electron excitation[22].

In Fig. 2a, we show two TERS spectra (red) obtained from the 'on-resonance' and 'off-resonance' conditions defined below. 'On-resonance' here refers to good spectral matching between the nanocavity plasmon resonance (blue curves) and the downward molecular vibronic transition of $Q_y(1,1)$. The latter has an energy similar to that of the $Q_y(0,0)$ band measured by the photoluminescence excitation technique (see brown curve at the bottom of Fig. 2a and the schematic of molecular vibronic transitions in Fig. 2b). In contrast, 'off-resonance' refers to the situation in which the nanocavity plasmon resonance does not match well with the $Q_y(1,1)$ band, but does match the laser line. We note that for H_2TBPP molecules, the laser line at 532 nm is always resonant with the upward molecular vibronic $Q_y(1,0)$ transition, but under the 'off-resonance' condition, the TERS spectrum shows very few observable spectral features. In contrast, a dramatic enhancement of the Raman signals can be observed under the 'on-resonance' condition even under a small incident laser flux of about 10^2 W cm^{-2}. The Raman vibrational modes appear as sharp spectral features on top of a smooth continuum, whose profile matches very well with the nanocavity plasmon profile.

In other words, under the 'on-resonance' condition, the broadband nature of the nanocavity plasmon field allows us to realize an efficient

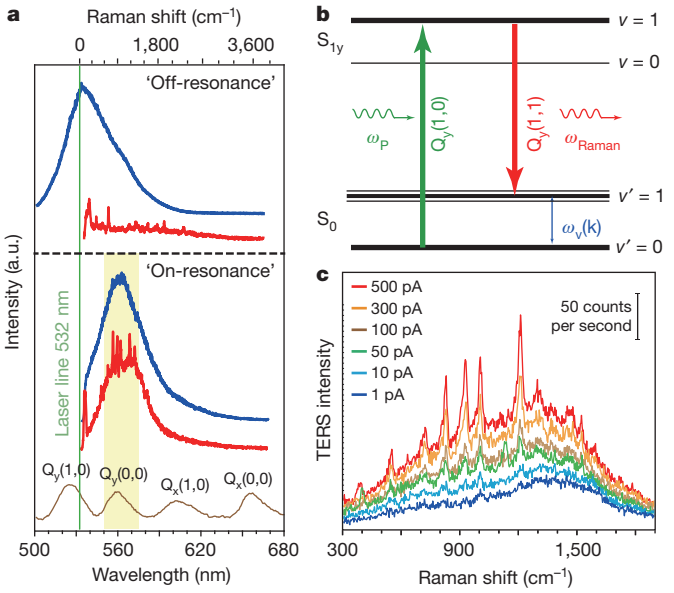

Figure 2 | Spectral matching to generate broadband nanocavity plasmon-enhanced Raman scattering. **a**, Dependence of TERS spectra (red, 200 mV, 1 nA, 3 s) on the spectral matching among the laser line (green), nanocavity plasmon resonance (blue), and molecular vibronic transitions (brown). The lower panel shows the 'on-resonance' situation with the nanocavity plasmon resonance matching the downward molecular vibronic transition $Q_y(0,0)$. The nanocavity plasmon profile (blue) is determined by STM-induced luminescence for the Ag tip on Ag(111) (2.8 V, 0.1 nA, 10 s), whereas the adsorption spectrum of H_2TBPP (brown) is measured by photoluminescence excitation. The upper panel shows the 'off-resonance' situation in which the nanocavity plasmon resonance does not match the downward $Q_y(0,0)$ transition. The scale on the top axis shows the Raman shifts for the TERS measurements. **b**, Schematic of the optical transitions involved in the Raman process between the ground state S_0 and excited state S_1, in which ω_P is the frequency of the incident pumping laser, ω_{Raman} is the frequency of Raman photons, and $\omega_v(k)$ is the vibrational frequency of the k_{th} mode of the molecule; v and v′ stand for the vibrational levels of excited states and ground states, respectively. **c**, TERS spectra on the molecular island as a function of tunnelling currents (120 mV, 3 s).

doubly resonant TERS process: not only producing sufficient resonant excitation through the spectral overlap between the nanocavity plasmon shoulder, the laser line, and the upward molecular vibronic transitions, but, more importantly, also generating large resonant emission enhancement owing to the good spectral matching of the nanocavity plasmon resonance to the downward molecular vibronic transitions. It is worth mentioning that the photon flux used for the 'on-resonance' TERS experiments is about one to two orders of magnitude smaller than what has been reported to date ($\sim 10^3 - 10^4$ W cm^{-2})[6,14,17,21], thus guaranteeing the sustainability of the single molecule during the measurements, that is, it will not be damaged.

Moreover, the broad continuum and associated TERS signals are found to be enhanced dramatically when tunnelling currents are increased (Fig. 2c)[17], which suggests a highly sensitive dependency of both signals on the gap distance (that is, on the local field enhancement) (Supplementary Fig. 4c)[25]. In our spectral-matching TERS, the nanocavity plasmon resonance mode is tuned mainly by modifying the tip status[22] while the strength of the nanocavity plasmon mode is controlled by the gap distance set by the tunnelling condition, particularly the tunnelling current. A sufficiently intense nanocavity plasmon field associated with a relatively short gap distance is important to yield pronounced TERS signals.

However, as shown in Fig. 2a, the proper setting of the nanocavity plasmon resonance to satisfy the 'on-resonance' condition is much more critical to achieve large enhancement and high signal levels. These observations correlate directly with how the nanocavity plasmon field is involved in the Raman scattering process. The overall spectral profile of the 'on-resonance' TERS spectrum in Fig. 2a strikingly resembles that in the broadband femtosecond stimulated Raman scattering process[28]. In addition, we also observed a nonlinear relationship between the TERS response and the incident laser power (see Supplementary Figs 4 and 5). Such nonlinear power dependency, together with the spectral profile similarity to the broadband stimulated Raman scattering, suggests that our spectral-matching TERS can be viewed as an analogue to the third-order nonlinear stimulated Raman scattering process[28], providing both enhanced signals and improved spatial resolution (see Supplementary Information for more details).

The large enhancement thus gained by exploiting the broadband nanocavity-plasmon-stimulated Raman process not only allows for non-invasive TERS measurements with single-molecule sensitivity, but also provides an opportunity to explore the influence of molecular orientations on the vibrational spectral features. Figure 3a shows two representative TERS spectra acquired on two isolated molecules with different adsorption configurations (or molecular orientations). As shown in the STM images on the right (which remain the same after the TERS measurements), one spectrum is acquired on a single flat-lying H_2TBPP molecule adsorbed on the terrace of Ag(111) (blue spectrum), and the other is on a single tilted molecule adsorbed at the step edge (red spectrum). Both spectra reveal vibrational fingerprints characteristic of the H_2TBPP molecules (Fig. 1c) in terms of Raman peak positions.

However, there also exist differences in the relative peak intensities between the two spectra in Fig. 3a, reflecting the changes in the adsorption configurations (or molecular orientations). With the help of the density functional theory calculations under the dipole approximation,

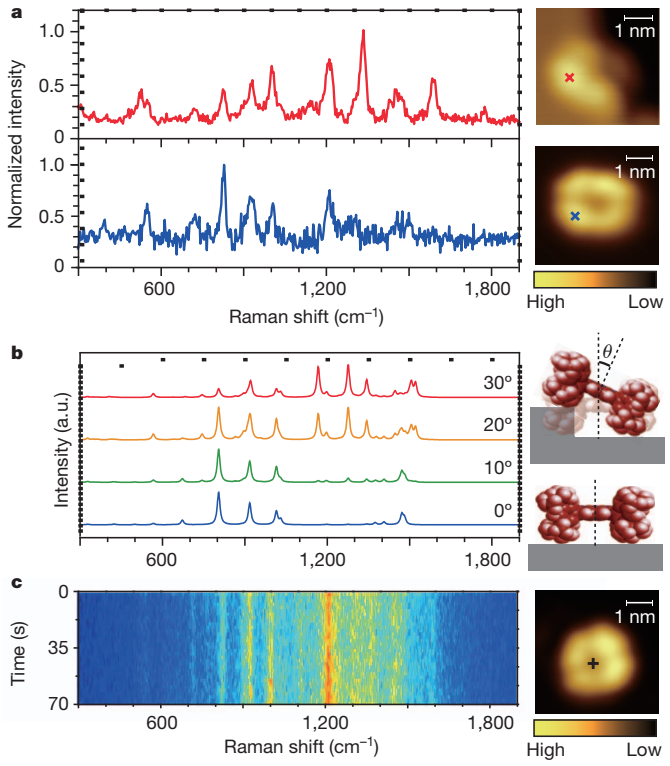

Figure 3 | Single-molecule TERS spectra and their dependency on molecular orientations. **a**, Single-molecule TERS spectra (100 mV, 1 nA, 3 s) for an isolated H_2TBPP molecule adsorbed on the terrace (bottom, blue) or at the step edge (top, red) of Ag(111). Both spectra were acquired on the molecular lobes marked with crosses in the STM images on the right (subtracted from the broad continuum for clarity). **b**, Calculated TERS spectra of a molecule for different tilt angles θ. Shown on the right are the schematics of flat-lying and tilted molecules, respectively. **c**, 35 sequential TERS spectra (120 mV, 1 nA, 2 s) acquired on the centre of a single flat-lying H_2TBPP molecule adsorbed on the Ag(111) terrace (the terrace is the flat area between the step edges); the centre is marked as a cross in the corresponding STM image on the right.

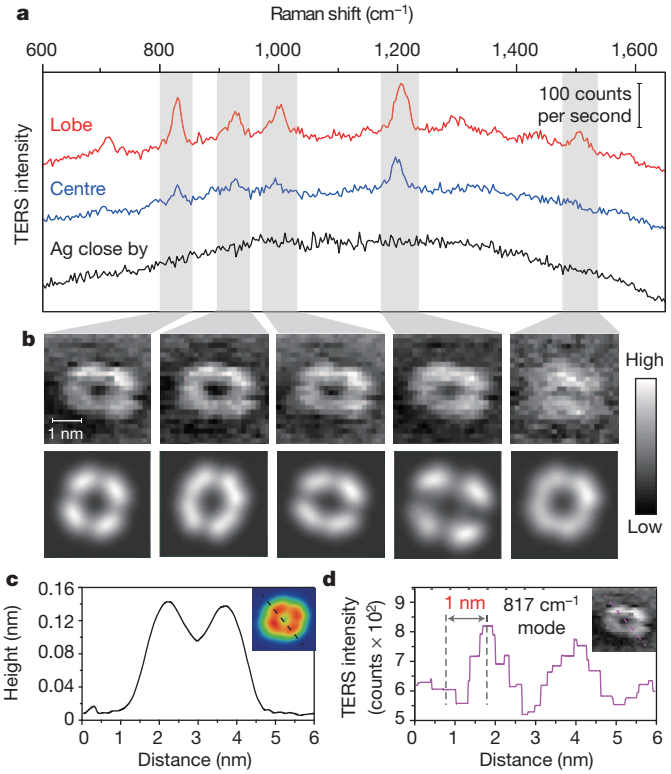

Figure 4 | TERS mapping of a single H_2TBPP molecule on Ag(111). **a**, Representative single-molecule TERS spectra on the lobe (red) and centre (blue) of a flat-lying molecule on Ag(111). The TERS spectrum on the bare Ag about 1 nm away from the molecule is also shown, in black (120 mV, 1 nA, 3 s). **b**, The top panels show experimental TERS mapping of a single molecule for different Raman peaks (23 × 23, ~0.16 nm per pixel), processed from all individual TERS spectra acquired at each pixel (120 mV, 1 nA, 0.3 s; image size: 3.6 × 3.6 nm^2). The bottom panels show the theoretical simulation of the TERS mapping. **c**, Height profile of a line trace in the inset STM topograph (1 V, 20 pA). **d**, TERS intensity profile of the same line trace for the inset Raman map associated with the 817 cm^{-1} Raman peak, integrated over 800−852 cm^{-1}.

the origin of such differences can be associated to the particular orientation of the single molecule that governs the Raman selection rules of the fingerprints. The simulated spectra in Fig. 3b correctly interpret the activation and deactivation of the experimental modes observed in Fig. 3a when the tilting angle of the molecule is changed (see Supplementary Methods for more information). As often found in experiments, similar spectral variations can also occur on the same molecule during the TERS measurements, owing to configurational changes, particularly under the strong illumination condition. Previous single-molecule TERS studies under ambient conditions are usually based on statistical analysis of such spectral fluctuations within a timescale of several seconds[6,7,9,10,17]. However, a single molecule can also remain stable for a certain period of time during the TERS measurements without revealing any substantial spectral changes.

Remarkably, Fig. 3c shows one example of such stability over 70 s when 35 sequential TERS measurements were made on a single H_2TBPP molecule on the Ag terrace. The STM image on the right was taken before the sequential TERS measurements, but remains the same after the measurements. Such molecular stability over a sufficiently long period of time is crucial to perform TERS imaging experiments that can yield a complete and meaningful spectral map.

The realization of efficient nanocavity-plasmon-stimulated Raman scattering in our STM-controlled technique provides a means of performing Raman mapping with unprecedented spatial resolution. Figure 4a indicates that, for an isolated single H_2TBPP molecule on Ag(111), the TERS spectra acquired on the molecular lobe are stronger than those on the centre, whereas the nearby Ag gives a broad continuum, highlighting the highly localized nature of the TERS signals. Such contrast is best illustrated in the panoramic TERS mapping image in Fig. 4b (top row), in which we plot experimental TERS mapping results of a flat-lying molecule on Ag for five selected Raman peaks. The characteristic four-lobe pattern of a H_2TBPP molecule is discernible in the TERS mapping, at least for low-wavenumber vibrational modes. The molecular lobes appear bright but the centre appears dark. However, for relatively large wavenumbers of 1,210 cm^{-1} or above, the contrast and central dark area become smaller.

Such Raman image contrast and frequency dependence can be qualitatively understood by the relative locality of the vibrational modes of the H_2TBPP molecule with respect to the axial polarization of the highly confined local plasmonic fields[6] (Supplementary Video). In brief, the low-wavenumber vibrational modes are more localized in the lobe while the high-wavenumber modes above about 1,210 cm^{-1} contain more contribution from the porphyrin core. To help to explain the contrast between these Raman images and their evolution, the bottom of Fig. 4b shows TERS mapping by assuming that the enhanced local electric field follows a Gaussian beam distribution (Supplementary Methods). The simulated images are consistent with the experimental TERS mapping results, although the consistency is better at low-wavenumber vibrational modes. Strikingly, in comparison with the spatial resolution of the STM topograph (Fig. 4c), the profile of the Raman spectral mapping shown in Fig. 4d not only exhibits a comparable spatial resolution below 1 nm (about 0.5 nm estimated within a 10% to 90% contrast), but more importantly, also provides chemically resolved information revealing intramolecular features.

The ability to access the structure and conformation of a single molecule with both chemical recognition and subnanometre resolution by optical means as presented here provides a new potential to explore the nanometre-scale world, offering new ways to design, control and engineer the functionality of molecules on demand. This should substantially affect the fields of nanophotonics, biochemistry, surface science and molecular electronics, in which identifying molecular species with single-molecule resolution is important. Furthermore, our findings open up a new avenue for studying nonlinear optical processes and photochemistry at the single-molecule scale.

METHODS SUMMARY

Our STM-controlled TERS experiments were performed on a custom low-temperature and ultrahigh-vacuum STM (Unisoku) in a confocal-type side-illumination configuration[29] at about 80 K under a base pressure of around 10^{-10} torr (Supplementary Fig. 1). H_2TBPP molecules were thermally evaporated onto the Ag(111) surface (previously cleaned by argon ion sputtering and annealing). Silver was also used as tip material because the nanogap defined by the Ag tip and the Ag substrate can offer very strong plasmonic resonance[30]. After fabrication via electrochemical etching, Ag tips were cleaned in ultrahigh vacuum via outgassing and ion sputtering, with the tip status further modified by high-voltage pulses[30]. STM imaging and spectral measurements were taken in a constant-current mode with the sample biased. The photon collection and detection systems were described previously[22,30]. A continuous-wave laser at 532 nm is used as a Raman pumping source with a photon flux of about 100 W cm^{-2} illuminating over the junction area.

Received 20 November 2012; accepted 25 March 2013.

1. Stöckle, R. M., Suh, Y. D., Deckert, V. & Zenobi, R. Nanoscale chemical analysis by tip-enhanced Raman spectroscopy. *Chem. Phys. Lett.* **318,** 131–136 (2000).
2. Anderson, M. S. Locally enhanced Raman spectroscopy with an atomic force microscope. *Appl. Phys. Lett.* **76,** 3130–3132 (2000).
3. Hayazawa, N., Inouye, Y., Sekkat, Z. & Kawata, S. Metallized tip amplification of near-field Raman scattering. *Opt. Commun.* **183,** 333–336 (2000).
4. Pettinger, B., Picardi, G., Schuster, R. & Ertl, G. Surface enhanced Raman spectroscopy: towards single molecular spectroscopy. *Electrochem. Jpn.* **68,** 942–949 (2000).
5. Anderson, N., Hartschuh, A., Cronin, S. & Novotny, L. Nanoscale vibrational analysis of single-walled carbon nanotubes. *J. Am. Chem. Soc.* **127,** 2533–2537 (2005).
6. Neacsu, C. C., Dreyer, J., Behr, N. & Raschke, M. B. Scanning-probe Raman spectroscopy with single-molecule sensitivity. *Phys. Rev. B* **73,** 193406 (2006).
7. Sonntag, M. D. *et al.* Single-molecule tip-enhanced Raman spectroscopy. *J. Phys. Chem. C* **116,** 478–483 (2012).
8. Berweger, S. *et al.* Optical nanocrystallography with tip-enhanced phonon Raman spectroscopy. *Nature Nanotechnol.* **4,** 496–499 (2009).
9. van Schrojenstein Lantman, E. M., Deckert-Gaudig, T., Mank, A. J. G., Deckert, V. & Weckhuysen, B. M. Catalytic processes monitored at the nanoscale with tip-enhanced Raman spectroscopy. *Nature Nanotechnol.* **7,** 583–586 (2012).
10. Liu, Z. *et al.* Revealing the molecular structure of single-molecule junctions in different conductance states by fishing-mode tip-enhanced Raman spectroscopy. *Nature Commun.* **2,** 305 (2011).
11. Alonso-González, P. *et al.* Resolving the electromagnetic mechanism of surface-enhanced light scattering at single hot spots. *Nature Commun.* **3,** 684 (2012).
12. Ichimura, T. *et al.* Subnanometric near-field Raman investigation in vicinity of a metallic nanostructure. *Phys. Rev. Lett.* **102,** 186101 (2009).
13. Steidtner, J. & Pettinger, B. Tip-enhanced Raman spectroscopy and microscopy on single dye molecules with 15 nm resolution. *Phys. Rev. Lett.* **100,** 236101 (2008).
14. Stadler, J., Schmid, T. & Zenobi, R. Nanoscale chemical imaging using top-illumination tip-enhanced Raman spectroscopy. *Nano Lett.* **10,** 4514–4520 (2010).
15. Yano, T., Verma, P., Saito, Y., Ichimura, T. & Kawata, S. Pressure-assisted tip-enhanced Raman imaging at a resolution of a few nanometres. *Nature Photon.* **3,** 473–477 (2009).
16. Treffer, R., Lin, X. M., Bailo, E., Deckert-Gaudig, T. & Deckert, V. Distinction of nucleobases—a tip-enhanced Raman approach. *Beilstein J. Nanotechnol* **2,** 628–637 (2011).
17. Pettinger, B., Schambach, P., Villagómez, C. J. & Scott, N. Tip-enhanced Raman spectroscopy: near-fields acting on a few molecules. *Annu. Rev. Phys. Chem.* **63,** 379–399 (2012).
18. Berweger, S. & Raschke, M. B. Signal limitations in tip-enhanced Raman scattering: the challenge to become a routine analytical technique. *Anal. Bioanal. Chem.* **396,** 115–123 (2010).
19. Xu, H. X., Aizpurua, J., Käll, M. & Apell, P. Electromagnetic contributions to single-molecule sensitivity in surface-enhanced Raman scattering. *Phys. Rev. E* **62,** 4318–4324 (2000).
20. Aizpurua, J., Hoffmann, G., Apell, S. P. & Berndt, R. Electromagnetic coupling on an atomic scale. *Phys. Rev. Lett.* **89,** 156803 (2002).
21. Jiang, N. *et al.* Observation of multiple vibrational modes in ultrahigh vacuum tip-enhanced Raman spectroscopy combined with molecular-resolution scanning tunneling microscopy. *Nano Lett.* **12,** 5061–5067 (2012).
22. Dong, Z. C. *et al.* Generation of molecular hot electroluminescence by resonant nanocavity plasmons. *Nature Photon.* **4,** 50–54 (2010).
23. Dong, Z. C. *et al.* Vibrationally resolved fluorescence from organic molecules near metal surfaces in a scanning tunneling microscope. *Phys. Rev. Lett.* **92,** 086801 (2004).
24. Stipe, B. C., Rezaei, M. A. & Ho, W. Single-molecule vibrational spectroscopy and microscopy. *Science* **280,** 1732–1735 (1998).
25. Pettinger, B., Domke, K. F., Zhang, D., Picardi, G. & Schuster, R. Tip-enhanced Raman scattering: influence of the tip-surface geometry on optical resonance and enhancement. *Surf. Sci.* **603,** 1335–1341 (2009).
26. Itoh, T. *et al.* Surface-enhanced resonance Raman scattering and background light emission coupled with plasmon of single Ag nanoaggregates. *J. Chem. Phys.* **124,** 134708 (2006).

27. Yorulmaz, M., Khatua, S., Zijlstra, P., Gaiduk, A. & Orrit, M. Luminescence quantum yield of single gold nanorods. *Nano Lett.* **12,** 4385–4391 (2012).
28. Kukura, P., McCamant, D. W. & Mathies, R. A. Femtosecond stimulated Raman spectroscopy. *Annu. Rev. Phys. Chem.* **58,** 461–488 (2007).
29. Wang, X. *et al.* Tip-enhanced Raman spectroscopy for investigating adsorbed species on a single-crystal surface using electrochemically prepared Au tips. *Appl. Phys. Lett.* **91,** 101105 (2007).
30. Zhang, C. *et al.* Fabrication of silver tips for scanning tunneling microscope induced luminescence. *Rev. Sci. Instrum.* **82,** 083101 (2011).

Supplementary Information is available in the online version of the paper.

Acknowledgements We thank B. Wang, B. Ren, H. X. Xu, Z. Liu, and X. M. Yang for discussions and Unisoku Company for technical assistance. This work is supported by the National Basic Research Program of China, the Strategic Priority Research Program of the Chinese Academy of Sciences, the Natural Science Foundation of China and the Basque Government Project of Excellence (ETORTEK).

Author Contributions R.Z. and Y.Z. contributed equally to this work. Z.C.D. and J.G.H. supervised the project and designed the experiments. R.Z., Y.Z., S.J., C.Z., L.G.C., L.Z., Y.L. and Z.C.D. performed experiments and analysed data. Y.Z., J.A., Y.L., J.L.Y. and Z.C.D. contributed to the interpretation of the data and theoretical simulations. Z.C.D., Y.Z., Y.L., J.A. and J.G.H. wrote the manuscript.

Author Information Reprints and permissions information is available at www.nature.com/reprints. The authors declare no competing financial interests. Readers are welcome to comment on the online version of the paper. Correspondence and requests for materials should be addressed to Z.C.D. (zcdong@ustc.edu.cn) and J.G.H. (jghou@ustc.edu.cn).